

Mixup Barcodes: Quantifying Geometric-Topological Interactions between Point Clouds

Hubert Wagner 

University of Florida, Gainesville, US

Nickolas Arustamyan 

University of Florida, Gainesville, US

Matthew Wheeler 

University of Florida, Gainesville, US

Peter Bubenik 

University of Florida, Gainesville, US

Abstract

We propose a novel geometric-topological descriptor called a mixup barcode. Intuitively, it characterizes the shape of a point clouds as well as its interaction with another point cloud embedded in the same space. More technically, it enriches a standard persistence barcode with information about the image persistent homology. In three dimensions it captures natural notions that could be called overlap, encirclement and surrounding; in higher dimensions more intricate, unnamed interactions are captured. We provide a theoretical setup as well as a novel algorithm for mixup barcodes.

As a proof of concept, we apply this tool to a geometric-topological problem arising from machine learning. We make first steps towards verifying a hypothesis stating that geometric-topological interactions within intermediate point cloud representations in an artificial neural network can hinder its training. More broadly, our experiments suggest that mixup barcodes are useful for characterizing spatial interactions that are hard to directly visualize or capture using standard methods.

2012 ACM Subject Classification F.2.2 Nonnumerical Algorithms and Problems; Theory of computation → Computational geometry; Mathematics of computing → Combinatorial algorithms

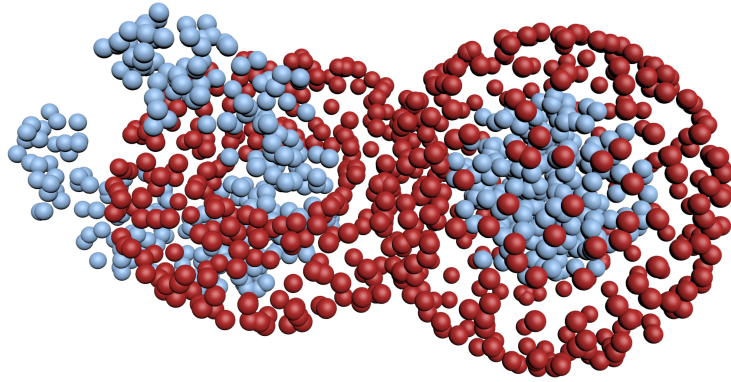
Keywords and phrases mixup barcode, persistent homology, persistence barcode, persistence diagram, image persistent homology, image persistence, deep learning, multi layer perceptron, topology of neural network embeddings, disentanglement

1 Introduction

Computational geometry delivers a variety of tools for characterizing the shape of a point cloud. One can compute the convex hull, the Delaunay triangulation and its variants, its subcomplexes such as the alpha shapes, its filtrations such as alpha complexes. Analogs for high dimensional point clouds such as Rips and Čech filtrations are becoming better understood [12] and more useful [2, 8].

In recent years, it become popular to summarize the geometric-topological structure of a point cloud using persistent homology. It involves computing a persistence diagram, or barcode, which serves as a geometric-topological descriptor of a dataset. Two datasets can be compared by matching their barcodes which yields a metric distance. Such comparison is invariant under translations and rotations of the data. While often useful, this invariance can be a limitation. This is especially true if the point clouds are embedded in the same space and geometric locations of their topological features play a role in the comparison.

General goal. We are interested in the following basic question:



■ **Figure 1** What are the shapes of the two point clouds and the spatial interactions between them? Would these interactions obstruct our attempt to separate, or *disentangle*, the two point clouds? Could we do this robustly, such that replacing these points with another sample would not cause problems? These are natural questions. Also, their high-dimensional generalizations play an important role in our application.

How can we characterize not only the shape of a point cloud, but also how it interacts with another point cloud embedded in the same space. See 1 for an example.

To answer this question, we propose a novel topological descriptor. In overview, our method computes how the inclusion of another point cloud affects the persistent homology of an existing point cloud. Specifically, we ask how the lifetime of each topological feature shortens in the presence of new data. This way we quantify the *geometric-topological interactions* between the two point clouds. While this task fits the general framework of multi-parameter persistent homology, we take a more pragmatic and computable approach. We frame this intuition in terms of persistent homology as well its variant, image persistent homology, which was recently shown to be efficiently computable [5]. We carefully combine these two pieces of information into a novel topological descriptor we call a mixup barcode.

A proof of concept application. Many high-dimensional problems in modern data science are geometric in nature and studying the topological properties of data is gaining popularity. We consider a problem arising in machine learning. We will refer to it as the *disentanglement problem*. In [22], it was hypothesized that training can be hindered by geometric-topological interactions within the intermediate representations (point clouds) produced by such models. Intuitively, a model may fail to **disentangle** the representations corresponding to data with different labels. First steps towards testing this hypothesis were recently made using persistent homology [20, 26]. We argue that our method is more suitable for this task, and present experiments supporting this claim. We elaborate on the setup in Section 7.

Contributions. The contributions of this paper include:

1. Theoretical foundation for a new topological descriptor called a *mixup barcode* characterizing interactions between point clouds.
2. A novel, practical algorithm for computing mixup barcodes.
3. Experiments showing the computability and usefulness of mixup barcodes in the above-mentioned machine-learning problem.
4. This is one of the first practical applications of image persistence [7] (which is a part of our construction) and the first we are aware of in the context of high-dimensional data.
5. One lesson learned is that persistence barcodes are unsuitable for such problems.
6. Software computing and visualizing the above concepts (to be released as open-source).

Purpose of this paper at SoCG. We hope to broaden the scope of basic geometric and topological problems discussed at SoCG. Specifically, many problems arising in modern data science, and particularly deep learning, are geometric in nature. Often, these are meta-problems related to understanding the emergent properties of machine learning algorithms. To solve such problems in a robust way, new foundational theory, algorithms and implementations are necessary. The SoCG community is uniquely equipped to develop all these aspects — and we hope that occasional papers like this one could help bridge the gap between our community and applied fields. This is a new direction, and also hope for expert feedback on the geometric, topological and algorithmic aspects of this work. We remark that the paper is submitted as the *Applications* paper type, which comes with its own review criteria.

Potential impacts. As for impacts within the SoCG community, we expect this work to expand the standard paradigm of topological data analysis, namely from summarizing and learning from the shape of a point cloud, to summarizing and learning from the *interactions* within point clouds. Our goals are aligned with the emerging direction of Chromatic Topological Data Analysis outlined in [10], although our work was developed independently.

Our method opens up applications in outside fields such as: cancer immunology (what are the spatial interactions between the tumor and immune-system cells?), protein docking (how do two proteins fit together?), material science (how do the atoms of one element fit with those of another?). In particular, our experiments suggest that the proposed methodology is applicable to geometric problems coming from machine learning.

2 Related work

We briefly review related work in computational geometry, topology as well as their relevant applications in machine learning.

Image persistence. Regarding computational methods for image persistence, an algorithm was proposed by Cohen-Steiner and collaborators [7]. An implementation is available in the first version of Morozov’s Dionysus library, but not in the current version. Recently, Bauer and Schmahl proposed a version [5] of the Ripser library for image persistence of Vietoris–Rips complexes, which informs our implementation. One of the first practical applications of image persistence was done recently in the context of image segmentation [23].

Cultrera di Montesano and collaborators [9] have proposed an approach for analyzing the mingling of a small number of 3-dimensional point clouds using image (as well as kernel and cokernel) persistence. One crucial development is the chromatic alpha complex which allows for the efficient computation of these variants of persistence for data embedded in low dimensions. Their motivation is similar to ours, although both projects were started and developed independently. Our focus is on a single descriptor combining standard persistence with image persistence, while theirs is on different types of persistent homology and connections between them. Natarajan et al, study the Morse theory of chromatic Delaunay complexes [21] and provide an implementation.

Induced matching. Our results are also related to work on induced matchings originating in [4]. In particular, similar ideas were independently explored by Gonzalez-Diaz and coauthors [14, 15, 25].

Disentanglement in deep neural networks. In machine learning, disentanglement is a broad concept. We are interested in how embeddings corresponding to different classes are separated during the training of a classifier. A motivation for this work goes back to an influential 2014 blog post [22] by Olah on "Neural Networks, Manifolds, and Topology" – ten years later we have appropriate computational tools to address this challenge.

Perhaps the first explicit mention of (manifold) disentanglement in the context of deep learning is in the work of Brahma, Wu and Yiyuan [6]. The work of Zhou and collaborators provides a topological view on disentanglement in the context of machine learning as well as a thorough overview [27]. We refer the reader interested in the machine learning details there, and focus on geometric-topological aspects of the problem. Our experiments are inspired by the work by Naitzat and collaborators [20] and the follow-up by Wheeler, Bouza and Bubenik [26]. We alleviate some of the shortcomings of these approaches that stem from the limitations of persistent homology (applied to a single point cloud).

3 Mixup barcodes

In this technical section we propose the mathematical setup for mixup barcodes. We delay detailed interpretation to the next section. We will work with filtrations of simplicial complexes, chain complexes, persistence modules and their decompositions. For brevity, we recall the standard definitions in Appendix A.

Let K denote a filtered finite simplicial complex $K_1 \hookrightarrow K_2 \hookrightarrow \dots \hookrightarrow K_n$ with inclusion maps $K_i \hookrightarrow K_j$ for $1 \leq i \leq j \leq n$, and similarly for L .

We will work with simplicial filtrations L and K under the assumption that for each $\sigma \in L_i$, $\sigma \notin K_{i-1}$, where $K_0 = \emptyset$. We further assume that our filtrations are simplex-wise, i.e. for each i , L_{i+1} differs from L_i by at most one simplex and similarly for K . The index of a simplex is the i at which it appears in the filtration, which is uniquely defined under the above assumptions.

We will sometimes assume that we have a real-valued order-preserving function f assigning a **filtration value** to each simplex. All the above assumptions arise naturally in the context of Vietoris–Rips filtrations, which will be our practical setup. We remark that everything in this section also generalizes to finite cell complexes.

The studied inclusion. For each $k \geq 0$ we consider the inclusion map $\iota : L \hookrightarrow K$ between our filtrations L and K . This gives rise to a variety of algebraic structures and induced maps between them, on which we elaborate in Appendix B. Of primary interest are the persistence modules $H_k(L)$ and $H_k(K)$ and an induced map between them $H_k(\iota) : H_k(L) \rightarrow H_k(K)$. This information is summarized in the following commutative diagram of vector spaces and linear maps.

$$\begin{array}{ccccccc}
 H_k(L_1) & \longrightarrow & H_k(L_2) & \longrightarrow & \dots & \longrightarrow & H_k(L_n) \\
 H_k(\iota_1) \downarrow & & H_k(\iota_2) \downarrow & & H_k(\iota_i) \downarrow & & H_k(\iota_n) \downarrow \\
 H_k(K_1) & \longrightarrow & H_k(K_2) & \longrightarrow & \dots & \longrightarrow & H_k(K_n)
 \end{array} \tag{1}$$

The image of the map of persistence modules in (1) is the following persistence module (and similarly for the kernel):

$$\text{im}(H_k(\iota)) = \text{im}(H_k(\iota_1)) \rightarrow \text{im}(H_k(\iota_2)) \rightarrow \dots \rightarrow \text{im}(H_k(\iota_i)) \rightarrow \dots \rightarrow \text{im}(H_k(\iota_n))$$

We are interested in the barcodes of the persistence module $H_k(L)$ (i.e. the persistent homology of L) and the persistence module $\text{im}(H_k(\iota))$ (i.e. the image persistent homology of the inclusion). Specifically, we will combine the information contained in these barcodes in a meaningful way, to form a single richer descriptor.

To do so, we notice that under our assumptions for each index $i \in \{1, 2, \dots, n\}$ there is at most one interval in the barcode with minimum value i . We call such i the **birth index** of

the corresponding interval in the barcode. This allows us to match these barcodes by the birth indices; for brevity we refer to the following more general result.

► **Theorem 1** (Matching [4, Theorem 4.2, Proposition 5.7]). *There is a canonical surjective matching from the barcode of $H_k(L)$ to the barcode of $\text{im}(H_k(\iota))$ which matches intervals with the same birth index.*

With this, we reorganize the information in this canonical matching of barcodes as follows.

► **Definition 2** (Mixup barcode). *The **mixup barcode** in degree k of the inclusion $L \hookrightarrow K$ is the collection of triples consisting of a triple (b, d', d) for each pair of matched intervals $[b, d]$ and $[b, d']$ in the barcodes of $H_k(L)$ and $\text{im}(H_k(\iota))$ and a triple (b, b, d) for each unmatched interval $[b, d]$ in the barcode of $H_k(L)$.*

The above definition is in terms of the filtration indices. In practice, we often replace them with the filtration values of the corresponding simplex. Typically the distinction will be clear from context, but sometimes we will explicitly talk about **index mixup barcodes**.

Viewing the mixup barcode as a refinement of the persistence barcode of L , we visualize it in a similar way. Specifically, we plot the image sub-bar in a light color, and its complement, the mixup sub-bar, in a darker color. We consider a separate mixup barcode for each degree, in practice 0, 1 and perhaps 2. See Figures 2, 3, 4 for examples.

Mixup barcodes for point clouds. We consider two finite point clouds, $A, B \subset \mathbb{R}^d$, or more generally, a finite metric space X with $A \subset X$ and $B = X \setminus A$, and construct Vietoris-Rips filtrations of A and $A \cup B$, with a common sequence of radii, $r_1 \leq r_2 \leq \dots \leq r_n$. The simplicial filtrations L and K are given by $L_i = \text{VR}(A; r_i)$ and $K_i = \text{VR}(A \cup B; r_i)$. By the mixup barcode of $A \hookrightarrow A \cup B$, we mean the mixup barcode induced by $L \hookrightarrow K$ as defined above. We stress than in this case a mixup barcode is a descriptor of *ordered* point clouds.

4 Related concepts and interpretation

With the main technical definition in place, we explain the rationale behind it, and mention some properties.

We start from defining an analog of a **persistence pair** [11] (storing birth and death) that can be expressed either in terms of the indices or filtration values.

► **Definition 3** (Mixup triple). *Each triple (b, d', d) in the mixup barcode of $L \hookrightarrow K$ is called an **mixup triple**.*

We reiterate what information is stored in each mixup triple.

► **Definition 4** (Persistence bar and image and mixup sub-bars). *For each mixup triple (b, d', d) , we have a **persistence bar** $[b, d]$, which splits into what we call:*

i an **image sub-bar** $[b, d']$, and

ii a **mixup sub-bar** $[d', d]$,

noting that degenerate sub-bars of the form $[x, x]$ are allowed.

► **Observation 1.** *For the mixup barcode of $L \hookrightarrow K$, the persistence bars give us the persistence barcode of L and the image sub-bars give us the image persistence barcode. However, the mixup sub-bars will generally not coincide with any bars of kernel persistence barcode. See Figure 2 for an explicit example.*

Premature death. Before we interpret the information captured by mixup barcodes, we recall the information captured by the persistent homology vector spaces of L , namely $\frac{Z_k(L_i)}{B_k(L_j) \cap Z_k(L_i)}$. Each bar $[b, d]$ in the resulting persistence barcode of L can be interpreted as the **birth** and **death** of a homology class in $H(L)$, namely the first index (or filtration value) at which it appears and the first at which it disappears, respectively.

► **Definition 5** (Premature death). *Given an index mixup triple (b, d', d) we interpret the index d' as the index of premature death of the unique homology class γ born at L_b . Specifically, we mean the first index at which γ becomes trivial or merges with an older homology class in $H_k(L)$.*

We remark that a premature death arises from the image persistent homology vector spaces of our inclusion, namely $\frac{Z_k(L_i)}{B_k(K_j) \cap Z_k(L_i)}$. It is therefore caused by the extra boundaries coming from K – but not by merging with another homology class absent from $H_k(L)$.

It should be clear that while the death can be premature, it cannot precede the birth:

► **Observation 2.** *For each mixup triple (b, d', d) in the mixup barcode we have $1 \leq b \leq d' \leq d \leq n + 1$.*

4.1 Statistics

It is often useful to extract a single number from a persistence barcode. For example, the total persistence – the sum of the lengths of all bars – is used to quantify the topological complexity of a point cloud. In a similar vein, we define simple ways of extracting a number to quantify the strength of interactions between filtrations L and K .

► **Definition 6** (Mixup). *The mixup of a mixup triple (b, d', d) is the value $d - d'$.*

In other words, it is the length of the sub-bar (d', d) which quantifies the prematurity of the death of a single homology class.

► **Definition 7** (Total mixup). *The total mixup of $L \hookrightarrow K$ is the sum of the mixups for the bars in the mixup barcode.*

In our visualization, it is simply the sum of the lengths of the dark bars. Equivalently, it is the difference between the total persistence of A and the total image persistence of $A \hookrightarrow A \cup B$. We will refer to this quantity as $\text{total-mixup}(A, B)$.

Scale invariant statistics. The next two definitions allow us to make scale-invariant measurements. Firstly, this allows us to compare data embedded in different dimensions. Secondly, the geometric scale of topological features is irrelevant in the context of our application.

► **Definition 8** (Mixup percentage). *The mixup percentage of mixup triple $t = (b, d', d)$ is*

$$\text{mixup\%}(t) = \frac{\text{mixup}(t)}{\text{pers}(t)} = \frac{d - d'}{d - b}. \quad (2)$$

► **Definition 9** (Total mixup percentage). *The total mixup percentage (mean mixup percentage) of a mixup barcode is the sum (mean) of the mixup percentages for all its bars.*

Note that the latter variant is between 0 and 1, but is *not* the ratio of the total mixup and the total persistence. The mean mixup percentage has the added benefit of allowing for the comparison between datasets of differing total persistence.

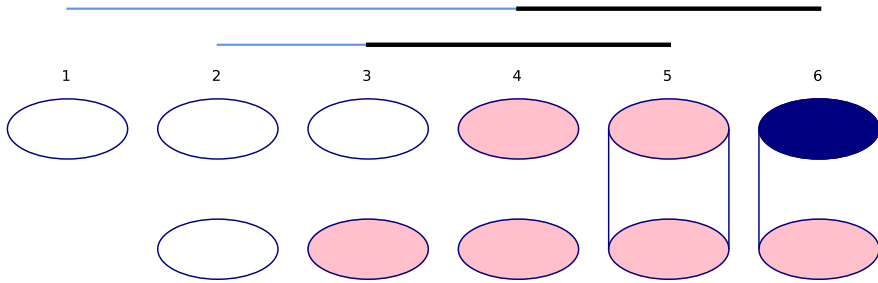


Figure 2 In this example K is a cylinder capped with disks. The dark cells (two circles, one disk and the cylinder) come from L , and the light cells (the two disks) come from $K \setminus L$. The new disk at L_6 is meant as another cell bounding the circle, distinct from the disk at K_4 (consistent with our assumptions). The mixup triples of $L \hookrightarrow K$ in degree 1 are $((1, 4, 6), (2, 3, 5))$, as illustrated with the mixup barcode plotted above. In particular, the mixup sub-bars $([4, 6], [3, 5])$ quantify the shortening of the lifetime of the two cycles. The kernel persistence bars are $([3, 6], [4, 5])$ are different and do not correspond to the shortening of the lifetimes of the cycles.

5 Examples and geometric interpretation

In this section we provide interpretations of the information captured by mixup barcodes in various degrees. It turns out that mixup barcodes capture intuitive geometric-topological interactions.

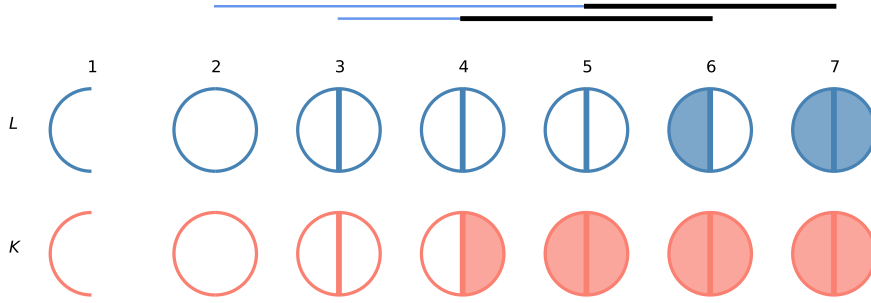
We recall that for a shape embedded in three dimensional space, homology groups in **degree 0, 1, 2** are often interpreted as various types of holes: the gaps between distinct parts of the object (or dually the connected components); tunnels (or handles); voids enclosed by the object. Note that in general voids correspond to H_{n-1} for objects in \mathbb{R}^n . Persistent homology captures the births and deaths of such features along the filtration.

Simple examples. Figure 2 shows a simple example (provided by a reviewer) using cell complexes. In particular, it illustrates that the mixup sub-bars capture the shortening of the lifetimes of homology classes. It also shows that the mixup sub-bars do not generally coincide with the kernel persistence bars. In such cases the kernel persistence bars do not have a clear interpretation, while the mixup bars do.

Figure 3 shows the behavior of a mixup barcode when cycle representatives of the generators of the persistence module $H_1(L)$ and $\text{im } H_1(\iota)$ are different. Namely if we label the cells arriving at L_1, L_2, L_3 as a, b, c , they are cellular chains $\{a+b, a+c\}$ and $\{a+b, b+c\}$, respectively. The premature death of the homology class of $a+c$ corresponds to the death of the class of $b+c$. We remark that these two classes share the birth simplex by construction.

Interpretation for point clouds. Going back to the case of a pair of point clouds A and B in \mathbb{R}^3 , the shortening of the lifetime of a homological feature conveys how points from B fill the holes of different types. Specifically, in degree 0, it quantifies to what extent the connected components in A merge quicker via points in B — which has natural interpretations as A and B **overlapping** or A being **separated** by B . In degree 1, it quantifies how points in B block a tunnel formed by A — or in other words how a portion of A encircles a portion of B . In degree 2, it quantifies how points in B are contained in the void created by A — which we interpret as A **surrounding** B . Figure 4 illustrates these interactions.

Intuitively, for point clouds in \mathbb{R}^n , the mixup barcode captures: **overlap** or **separation** in degree 0, **encirclement** in degree 1, and **surrounding** in degree $n-1$. In remaining



■ **Figure 3** This example is presented differently. The top filtration is L and the bottom filtration is K . The 1-cells are half-circles and a segment, and the 2-cells are half-disks. We assume that the cells added to L_6 and L_7 are distinct from the cells added in K_5 and K_4 . We consider the mixup barcode of $L \hookrightarrow K$ in degree 1.

degrees it captures more subtle, unnamed interactions.

6 Algorithm

In this section we describe an algorithm computing the decomposition of a persistence barcode into a mixup barcode and prove its correctness under the assumptions in Section 3. We start by recalling the algorithms for standard and image persistent homology, which will be part of our construction. Additionally, we provide an intuitive explanation of the latter algorithm, which is missing from its original description [7].

Standard reduction algorithm. We outline the standard algorithm for persistent homology, and then extend it to our setup. This algorithm performs a Gaussian elimination on the boundary matrix representing the filtration [11]:

■ Algorithm 1 Reduction algorithm for persistent homology

```

1: for  $j = 1$  to number of columns in  $R$  do
2:   while there exists a column  $k < j$  such that  $\text{pivot}(R[k]) = \text{pivot}(R[j])$  do
3:      $R[j] = (R[j] + R[k]) \text{ mod } 2$ 

```

The ordering of columns and rows corresponds to the order in which the elements (typically simplices) appear in the filtration. By adding the columns modulo 2, the algorithm removes conflicts between columns, understood as columns having the same pivot. The index persistence pairs are formed by the indices of nonzero columns and their pivots.

Elder rule and successor rule. Reordering the columns in the input boundary matrix would correspond to another filtration, in which the simplices arrive in a different order. However, reordering the rows has a more subtle effect. We interpret such reordering as the choice of the rule determining which homology class dies if two classes are merged. By definition, the older class survives and the younger dies. This is often called the **elder rule** [11]. In the algorithm, this decision is made by removing conflicts between the pivots, namely the greatest indices of a nonzero element in the columns. However, the standard algorithm can be modified to consider other merging rules, which we call **successor rules**.

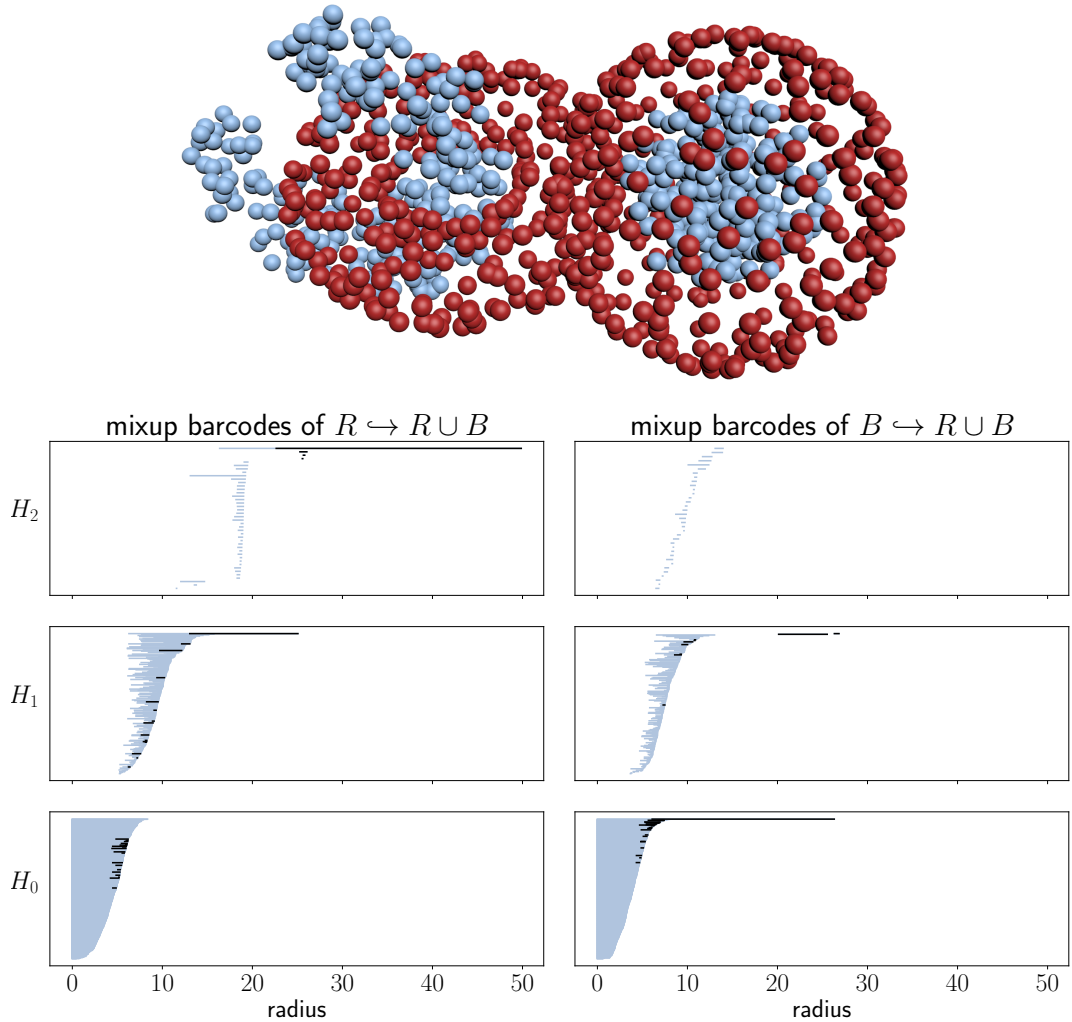


Figure 4 Top: Two point clouds: R red (dark) and B blue (light). Each samples two objects embedded in \mathbb{R}^3 with nontrivial topology interacting in nontrivial ways. **Bottom:** Mixup barcodes of R and B included in their union, in degrees 2, 1, 0. **Bottom left:** In H_2 , we see a prominent persistence bar with a long mixup bar. It detects the red **void** partially filled by blue points, interpreted as the red object **surrounding** a part of the blue object. Similarly in H_1 the prominent mixup bar detects the red handle (tunnel) that **encircles** the blue points. No significant mixup occurs in H_0 , although the many shorter mixup bars detect the **overlap** between the two shapes. **Bottom right:** In H_1 the mixup barcode detects the handle **encircled** by the red object, with the late birth indicating that a large part is missing. The prominent bar for H_0 detects that the two blue connected components connect quicker via the red points. We interpret this as **separation** of the two blue parts by the red object. As expected, there is no prominent persistence or mixup in H_2 .

► **Definition 10** (Successor rule). A *successor rule* decides which class is destroyed when two homology classes γ, κ become homologous.

For example, one could destroy the older class, which can be implemented by removing conflicts between the *smallest* nonzero indices (and not the largest ones). More generally, reordering the rows in the boundary matrix and using the standard reduction algorithm can be viewed as an implementation of a successor rule different than the standard elder rule.

Image persistent homology computations. The above perspective gives an interpretation of the algorithm for image persistent homology presented in [7, pp. 5-6]. The algorithm reorders the rows of the boundary matrix, so that the elements from L come first (ordered by the filtration index), followed by the elements from $K \setminus L$ (also ordered by the filtration index). The image index persistence pairs are of the form (σ, τ') , where the τ' is the index of a nonempty column whose pivot σ corresponds to a simplex in L [7, Observations (ii),(iii)]. This can be reinterpreted as using a successor rule that destroys the youngest class from $K \setminus L$ whenever available; otherwise, it destroys the youngest class from L , as usual.

Mixup barcodes algorithm. Algorithm 2 outlines the algorithm that decomposes the bars in the standard persistence diagram into the mixup barcode. The key new idea is to coordinate the two matrix reduction steps: for standard and image persistence. The latter computation involves the reordering of the rows mentioned above. This coordinated reduction allows us to merge the two pieces of information. In contrast, computing the standard and image persistence separately loses the correspondence between these two pieces of information. It also loses the crucial information about the mixup (which as we showed is not recoverable using kernel persistence).

Computational complexity and implementation. Due to the use of Gaussian elimination, the algorithm runs in $O(n^3)$ worst-case time, where n is the number of simplices in the filtration. As with standard persistence [3], the running time is significantly better in practice. With Matja Čufar, we developed an efficient implementation of the above algorithm within his ripserer framework [8]. The details of this implementation will be presented in another paper.

■ **Algorithm 2** Algorithm for Mixup Barcode in degree k

Require: Simplex-wise filtrations L and K as in Section 3; f assigning the filtration value to each simplex; degree k

- 1: BK = matrix with columns containing the boundaries of the k - and $(k+1)$ -simplices of K with rows and columns ordered by the filtration index
- 2: reorder the rows of BK such that the simplices from L have smaller indices than the simplices of $K \setminus L$ while retaining the relative order of simplices in L and also in $K \setminus L$
- 3: form matrix BL by zeroing out the entries in BK involving only the simplices of $K \setminus L$
- 4: reduce BL and BK using Algorithm 1
- 5: **for** each index σ of a k -simplex in L such that $BL[\sigma] = 0$ **do**
- 6: find τ such that $\text{pivot}(BL[\tau]) = \sigma$
- 7: find τ' such that $\text{pivot}(BK[\tau']) = \sigma$
- 8: $\text{birth} = f(\sigma)$; $\text{death} = \text{death}' = \infty$
- 9: **if** τ exists **then**
- 10: $\text{death} = f(\tau)$
- 11: **if** τ' exists **then**
- 12: $\text{death}' = f(\tau')$
- 13: record mixup triple $(\text{birth}, \text{death}', \text{death})$
- 14: return all the recorded mixup triples

► **Theorem 11** (Mixup Decomposition Theorem). *The algorithm in Algorithm 2 returns a correct mixup barcode of $L \hookrightarrow K$.*

Due to space constraints the proof is in Appendix C.

7 Application

We apply our method to analyzing high-dimensional point clouds. They come from a geometric problem arising from machine learning. The goal is to gain insights about the training of an artificial neural network [1] often called the **multi-layer perceptron** (MLP). It is the simplest *deep learning* method, often used for classification. We remark that models based solely on MLPs can achieve state of the art performance on challenging tasks [24]. In Appendix D we provide background on MLPs.

Model parameters. We use a 5-layer MLP, with embedding dimensions 512, 256, 128, 10 and L , where L depends on the number of considered labels (in our case 3 or 10). The model has $565,248 + 10L$ trainable parameters (weights).

7.1 Experiments

We use the new method to analyze geometric data arising from a machine learning model. The goal is to quantify geometric-topological difficulties during training – as theoretically outlined by Olah [22]. The results highlight the usefulness of the new methodology – especially in comparison to existing applications of persistent homology [20, 26] that were limited to quantifying the shape of a single point cloud.

In geometric terms, such a model learns a sequence of linear transformations each followed by a projection onto the positive orthant of \mathbb{R}^m , where m may be different at each step. This is done in an iterative training process, whose goal is to finally embed each input point with label l near the l -th standard basis vector.

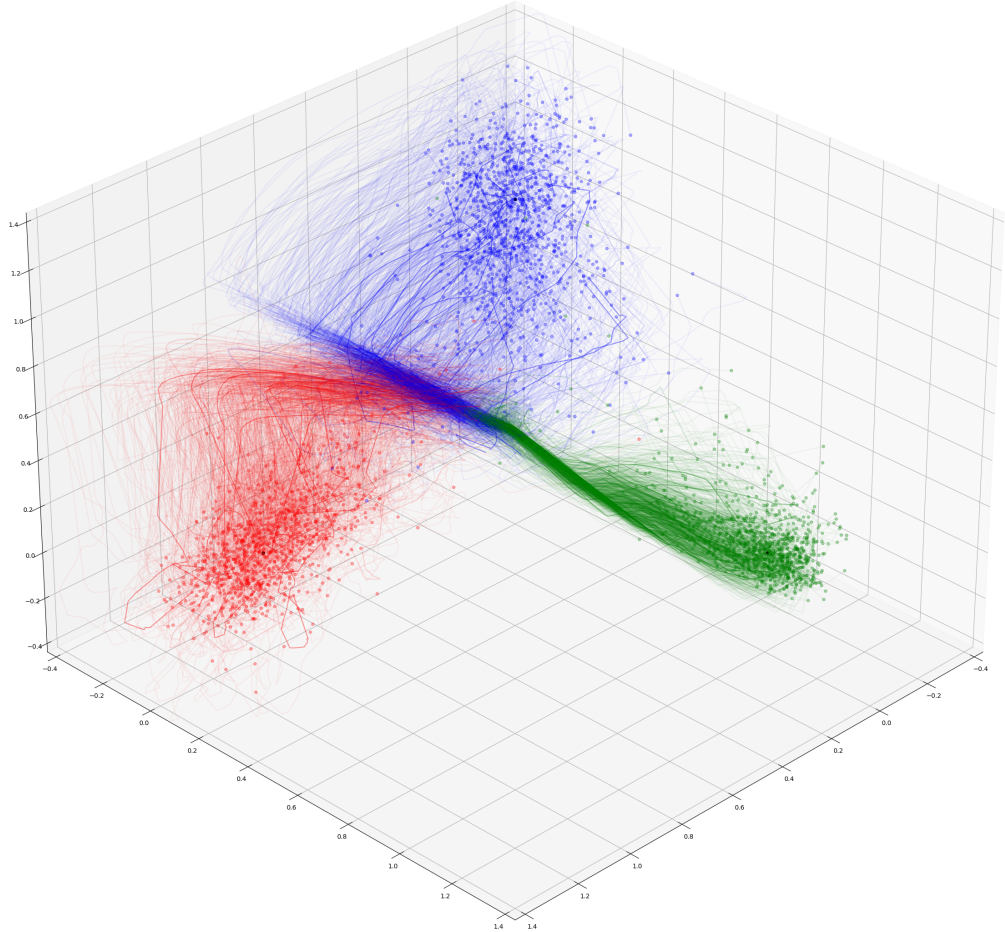


Figure 5 The three point clouds are the (soft) predictions produced by a trained machine learning model for three different classes of examples. The trajectories track the predictions during training, starting from a random state. We stress this does *not* show the disentanglement process directly, as it occurs in high dimensions as the data passes through the layers. It does show the evolution of the output of the last layer.

Goals. We consider the intermediate representation of the data produced by the i initial layers of the model, namely $M_i = L_i \circ L_{i-1} \circ \dots \circ L_1$. Given a single input vector v , we consider $(M_i(v))_i$, namely the sequence of embeddings of v produced by each M_i . Extending this to the entire input point cloud, we get a sequence of point clouds — which additionally change as training progresses. Figure 5 visualizes this information for the last layer of a model.

We analyze how the representation of input data disentangles passing through the layers — and track this process during training. We aim to verify the conjecture that complicated spatial interactions can hinder training.

Intuitively, a model can learn to perfectly disentangle the training labeled point cloud,

but still fail. For example, consider Figure 4. The model could learn a sequence of moves that take each blue point outside of the red points surrounding it. However, applying the same moves to a different sample (e.g. test data) will generally fail, since the red points sample a sphere and (some of) the blue points are inside it. As a result some of the red points may inadvertently be moved to the wrong location along with the blue points, resulting in misclassification.

The above situation is of course idealized. Additionally, the intermediate embedding dimensions can be arbitrarily high – and can exceed the dimension of the input data, meaning that any tangle can – in principle – be untangled. In particular, already in four embedding dimensions, the blue points can escape. Still, complicated entanglement is hypothesised [22,27] to correlate with training difficulties such as over-fitting and lack of generalization. Indeed, even if disentanglement is theoretically possible, it does not mean that the simplistic training process can realize it.

Datasets. To train the model, we will be using two datasets MNIST (easier, 99% accuracy) and CIFAR10 (harder, 76% accuracy). See Appendix E for more details. After training, we consider the embeddings produced from the test data. We treat the datasets as a finite labeled point cloud in $X \subset \mathbb{R}^d$. By X_i we mean **class** i of dataset X , namely the subset of points with label i .

Subsampling. Computing image persistence turns out to be generally slower ¹ than computing standard persistence for data of similar size and complexity [5]. We subsample A with 500 points and B with 100 points. We subsample consistently for all timesteps and layers. In degree 0, we use all available points.

► **Lemma 12** (Subsampling Property). *Given point clouds A , B and $B' \subset B$, $\text{total-mixup}(A, B') \leq \text{total-mixup}(A, B)$ (similarly for the mixup-percentage).*

Proof. While the birth and death of a homology class arising from A is unaffected by B , its premature death can only be *delayed* by using a subsample of B . Indeed, there are fewer boundaries coming from $\text{VR}(A \cup B'; r)$ than from $\text{VR}(A \cup B; r)$ that can shorten its life. ◀

In other words we only risk that the captured signal will be weaker.

To subsample, we can therefore safely use the k-medoids algorithm [16], the long-lost sibling of the popular k-means clustering [18]. Unlike k-means, it ensures that the cluster centers belong to the input point cloud, so we can indeed use it for subsampling. It was used in a similar context by Li and collaborators [17]. It is a good choice also in our case, because it is not crucial to carefully represent the shape of the points in B , since it has no bearing on the result. However, we aim to preserve the outliers. Indeed, even a single point in B surrounded by points in A may have a large impact on the topological mixup between A and B .

7.2 Why mixup and not persistence?

While our primary focus is to analyze the model (and not the input data), we mention a fact regarding the raw MNIST data. We stress this because previous studies considered the disentanglement of different classes of this dataset [26] computing the persistent homology of this data. It is however easy to check that the classes are pairwise linearly separable, except for a few outliers, making it unlikely that pairs of point clouds are entangled in complicated

¹ This issue is largely alleviated in our new implementation.

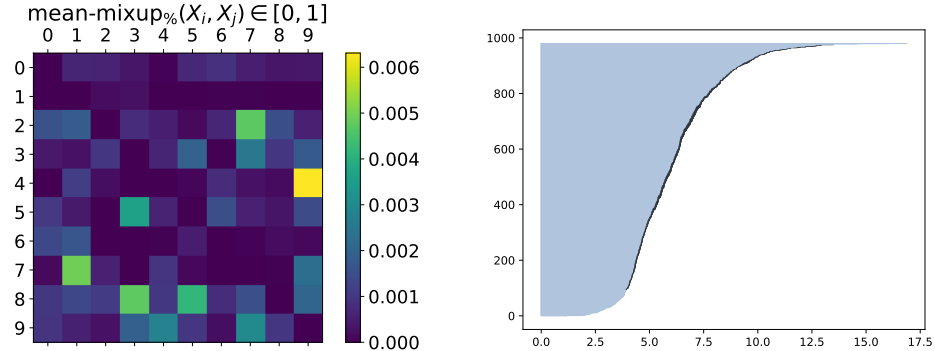


Figure 6 Left: The mean mixup percentage between all pairs of MNIST classes. Most values are low, as expected due to linear separability. **Right:** The mixup barcode between the images of fours and nines which achieve the greatest mixup. Many bars with small – but positive – mixup suggest that the two point clouds overlap along a long but shallow interface.

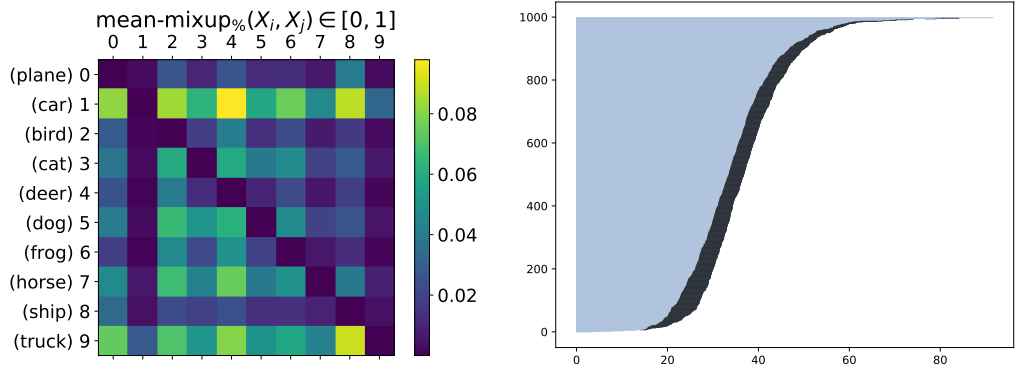


Figure 7 Left: The mean mixup percentage between all pairs of CIFAR10 classes. Note that the values are generally an order of magnitude higher than for the other dataset, with the highest value of 0.09 between classes 1 (airplane) and 4 (deer). **Right:** The mixup barcode between classes 1 and 4, suggesting a significantly more robust overlap than we saw in the other dataset.

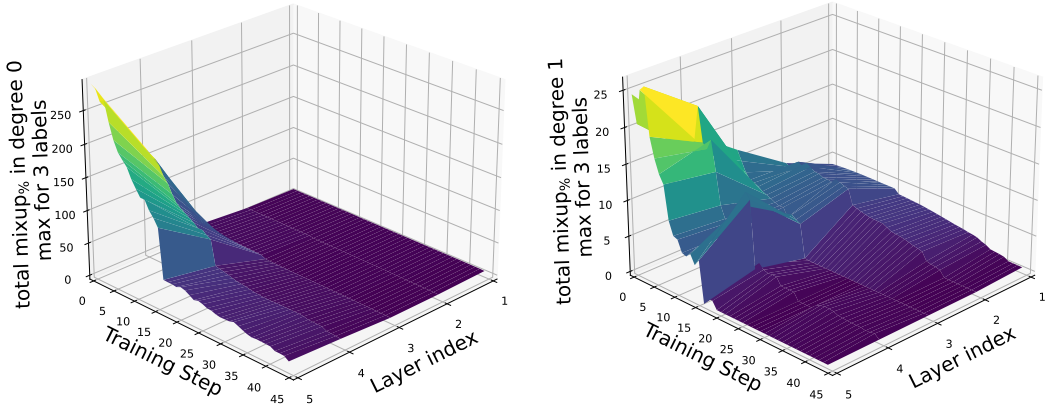
ways. As a sanity check, we verify that despite complicated topology, the mixup (which we use as a proxy for entanglement) is typically low in this case.

Specifically, we compute the mean percentage mixup in degree 0 for all pairs of classes of examples, namely for $A = X_i$ and $B = X_j$ for all $0 \leq i, j < 10$. The results for MNIST and CIFAR10 are in Figures 6 and 7. As expected, CIFAR10 exhibits greater mixup, often by an order of magnitude.

We emphasize that in general persistent homology of the data may be complicated, even if the point clouds are completely separated. Using persistence information directly would overestimate the amount of entanglement. The extra information about the mixup provided by our method is therefore important.

7.3 Disentanglement across layers

We track disentanglement across layers during training by analyzing a labeled point cloud $X_{kqt} \subset \mathbb{R}^n$ for each layer k ($1 \leq k \leq 5$), training step t , and label q ($1 \leq q \leq 3$).



■ **Figure 8** Mixup profiles characterizing the training on the MNIST dataset, in degree 0 (left) and degree 1 (right). We recall that the height corresponds to the mixup — the complexity of geometric-topological interactions — between intermediate embeddings of data with different labels at a given training step and layer of the model. Here, the mixup drops across layers and through successive training iterations, reflecting that the network successfully *disentangles* all the embeddings.

► **Definition 13** (Mixup profile). *At each layer k and time-step t , the mixup profile is computed as: $P_{kt} = \max_j \{ \text{total-mixup\%}(X_{kjt}, \bigcup_{r \neq j} X_{krt}) \}$, in degrees 0 and 1.*

The mixup profile P_{kt} measures complexity and strength of interactions between data representations with different labels, serving as a proxy for entanglement. It is visualized as a surface plot, with k and t on the horizontal axes and P_{kt} as the height.

Outcomes. See Figures 8 and 9 for a direct visualization of the mixup profiles for the MNIST and CIFAR datasets.

The main observation is that the mixup profiles are significantly different for the intermediate representations of the two datasets, suggesting that the interactions captured by the mixup barcodes indeed correlate with training difficulties.

Outcomes summary. The mixup profiles successfully distinguish between the training on the CIFAR and MNIST datasets. In particular, the mixup quickly drops for the easier dataset (MNIST), and not for the harder dataset (CIFAR). Overall, the statistics derived from the mixup barcodes do correlate with difficulties during training. They therefore support the conjecture stated in [22]. We stress that while MNIST and CIFAR10 are simple datasets, we analyze the training process on these datasets — which is poorly understood, even for these datasets.

8 Discussion

We presented a novel geometric-topological descriptor called a mixup barcode, and its summary statistics. Unlike persistence barcodes, mixup barcodes can be used to characterize not only the shape of a dataset but also its interactions with other datasets. Our work complements recent development of **Chromatic TDA**, an emerging branch of computational geometry and topology [10].

On the applied side, this new tool shed some light on the complicated geometry of the training process of a machine learning model. The experiments suggest that the theoretical

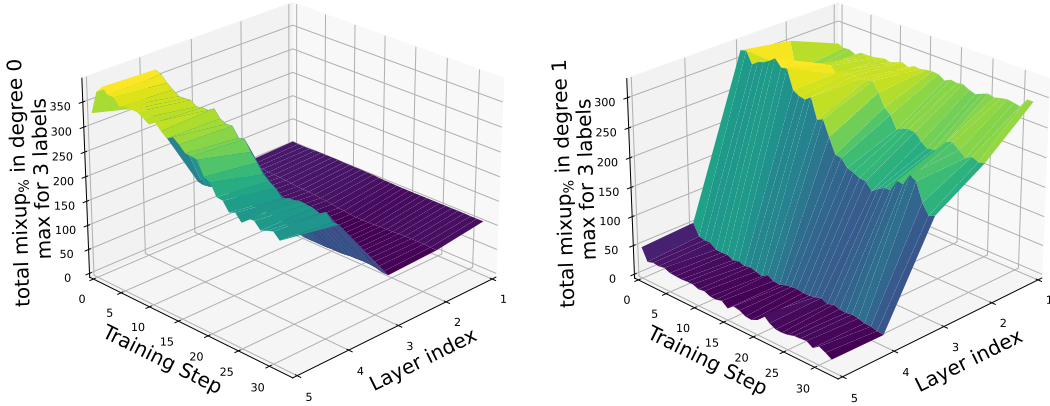


Figure 9 Mixup profiles characterizing the training on the more challenging CIFAR dataset. The total mixup percentage is generally much higher for CIFAR as compared to MNIST. This is consistent with the worse performance of this model on the CIFAR dataset. The graphs suggest that the information captured in the mixup barcodes does indeed correlate with training difficulties and the models failure to disentangle the embeddings.

considerations proposed in [22] can now be realized computationally. The main outcome is that this method can capture spatial interactions that were conjectured to hinder training [22]. We expect that this new tool could help detect problems – such as overfitting – already during training, or regularize (or otherwise better control) the training to avoid such problems altogether.

References

- 1 Shunichi Amari. A theory of adaptive pattern classifiers. *IEEE Transactions on Electronic Computers*, EC-16(3):299–307, 1967. doi:10.1109/PGEC.1967.264666.
- 2 Ulrich Bauer. Ripser: efficient computation of vietoris–rips persistence barcodes. *Journal of Applied and Computational Topology*, 5(3):391–423, 2021.
- 3 Ulrich Bauer, Michael Kerber, Jan Reininghaus, and Hubert Wagner. Phat: Persistent homology algorithms toolbox. *Journal of Symbolic Computation*, 78:76 – 90, 2017. Algorithms and Software for Computational Topology. URL: <http://www.sciencedirect.com/science/article/pii/S0747717116300098>, doi:10.1016/j.jsc.2016.03.008.
- 4 Ulrich Bauer and Michael Lesnick. Induced matchings and the algebraic stability of persistence barcodes. *Journal of Computational Geometry*, 6(2):162–191, 2015.
- 5 Ulrich Bauer and Maximilian Schmahl. Efficient computation of image persistence. In *39th International Symposium on Computational Geometry (SoCG 2023)*. Schloss Dagstuhl-Leibniz-Zentrum für Informatik, 2023.
- 6 Pratik Prabhanjan Brahma, Dapeng Wu, and Yiyuan She. Why deep learning works: A manifold disentanglement perspective. *IEEE Transactions on Neural Networks and Learning Systems*, 27(10):1997–2008, 2016. doi:10.1109/TNNLS.2015.2496947.
- 7 David Cohen-Steiner, Herbert Edelsbrunner, John Harer, and Dmitriy Morozov. Persistent homology for kernels, images, and cokernels. In *Proceedings of the twentieth annual ACM-SIAM symposium on Discrete algorithms*, pages 1011–1020. SIAM, 2009.
- 8 Matija Čufar. Ripserer. jl: flexible and efficient persistent homology computation in julia. *Journal of Open Source Software*, 5(54):2614, 2020.
- 9 Sebastiano Cultrera di Montesano, Ondřej Draganov, Herbert Edelsbrunner, and Morteza Saghafian. Persistent homology of chromatic alpha complexes. *arXiv preprint arXiv:2212.03128*, 2022.

- 10 Sebastiano Cultrera di Montesano, Ondrej Draganov, Herbert Edelsbrunner, and Morteza Saghafian. Chromatic topological data analysis. *arXiv preprint arXiv:2406.04102*, 2024.
- 11 Herbert Edelsbrunner and John Harer. *Computational topology: an introduction*. American Mathematical Soc., 2010.
- 12 Herbert Edelsbrunner and János Pach. Maximum betti numbers of čech complexes. In *40th International Symposium on Computational Geometry (SoCG 2024)*. Schloss Dagstuhl–Leibniz-Zentrum für Informatik, 2024.
- 13 Kunihiko Fukushima. Visual feature extraction by a multilayered network of analog threshold elements. *IEEE Transactions on Systems Science and Cybernetics*, 5(4):322–333, 1969. doi: [10.1109/TSSC.1969.300225](https://doi.org/10.1109/TSSC.1969.300225).
- 14 Rocío González-Díaz, Marta Soriano-Trigueros, and Alejandro Torras-Casas. Additive partial matchings induced by persistence morphisms. *arXiv preprint arXiv:2006.11100*, 2020.
- 15 Rocío González-Díaz, Marta Soriano-Trigueros, and Álvaro Torras-Casas. Partial matchings induced by morphisms between persistence modules. *arXiv preprint arXiv:2107.04519*, 2021.
- 16 Leonard Kaufman and Peter J. Rousseeuw. Partitioning around medoids (program pam). In *Wiley Series in Probability and Statistics*, pages 68–125. John Wiley & Sons, Inc., Hoboken, NJ, USA, 1990. Retrieved 2021-06-13. doi: [10.1002/9780470316801.ch2](https://doi.org/10.1002/9780470316801.ch2).
- 17 Lei Li, Linda Yu-Ling Lan, Lei Huang, Congting Ye, Jorge Andrade, and Patrick C Wilson. Selecting representative samples from complex biological datasets using k-medoids clustering. *Frontiers in Genetics*, 13:954024, 2022.
- 18 J. B. MacQueen. Some methods for classification and analysis of multivariate observations. In *Proceedings of 5th Berkeley Symposium on Mathematical Statistics and Probability*, volume 1, pages 281–297. University of California Press, 1967. Retrieved 2009-04-07. URL: <https://projecteuclid.org/euclid.bsmsp/1200512992>.
- 19 Vinod Nair and Geoffrey E Hinton. Rectified linear units improve restricted boltzmann machines. In *Proceedings of the 27th international conference on machine learning (ICML-10)*, pages 807–814, 2010.
- 20 Gregory Naitzat, Andrey Zhitnikov, and Lek-Heng Lim. Topology of deep neural networks. *The Journal of Machine Learning Research*, 21(1):7503–7542, 2020.
- 21 Abhinav Natarajan, Thomas Chaplin, Adam Brown, and Maria-Jose Jimenez. Morse theory for chromatic delaunay triangulations. *arXiv preprint arXiv:2405.19303*, 2024.
- 22 Chris Olah. Neural Networks, Manifolds, and Topology, 2014. Accessed: 2024-06-28. URL: <http://colah.github.io/posts/2014-03-NN-Manifolds-Topology/>.
- 23 Nico Stucki, Johannes C Paetzold, Suprosanna Shit, Bjoern Menze, and Ulrich Bauer. Topologically faithful image segmentation via induced matching of persistence barcodes. In *International Conference on Machine Learning*, pages 32698–32727. PMLR, 2023.
- 24 Ilya O Tolstikhin, Neil Houlsby, Alexander Kolesnikov, Lucas Beyer, Xiaohua Zhai, Thomas Unterthiner, Jessica Yung, Andreas Steiner, Daniel Keysers, Jakob Uszkoreit, et al. Mlp-mixer: An all-mlp architecture for vision. *Advances in neural information processing systems*, 34:24261–24272, 2021.
- 25 Álvaro Torras-Casas, Eduardo Paluzo-Hidalgo, and Rocío González-Díaz. Topological data quality via 0-dimensional persistence matchings. *arXiv preprint arXiv:2306.02411*, 2023.
- 26 Matthew Wheeler, Jose Bouza, and Peter Bubenik. Activation landscapes as a topological summary of neural network performance. In *2021 IEEE International Conference on Big Data (Big Data)*, pages 3865–3870. IEEE, 2021.
- 27 Sharon Zhou, Eric Zelikman, Fred Lu, Andrew Y Ng, Gunnar E Carlsson, and Stefano Ermon. Evaluating the disentanglement of deep generative models through manifold topology. In *International Conference on Learning Representations*, 2020.

A Preliminaries

We recall basic concepts from algebraic and computational topology. We will work with filtrations of simplicial complexes, chain complexes, persistence modules and their decompositions.

For a simplicial complex K , and $k \geq 0$, let $C_k(K)$ denote the \mathbb{Z}_2 -vector space whose basis is the set of k -simplices in K . Let $d_k : C_k(K) \rightarrow C_{k-1}(K)$ denote the differential, where $C_{-1}(K) = 0$. $(C_k(K), d_k)_{k \geq 0}$ is called the simplicial chain complex of K and denoted $C(K)$ for short. Let $Z_k(K) = \ker(d_k)$, $B_k(K) = \text{im}(d_{k+1})$ and $H_k(K) = \ker(d_k) / \text{im}(d_{k+1})$. $H_k(K)$ is called the simplicial homology of K in degree k . An inclusion of simplicial complexes $i : L \hookrightarrow K$ induces a chain map $C(i) : C(L) \rightarrow C(K)$ consisting of linear maps $C_k(i) : C_k(L) \rightarrow C_k(K)$ for each $k \geq 0$ such that for all k , $d_k \circ C_k(i) = C_{k-1}(i) \circ d_k$, where $C_{-1}(i) = 0$. It follows that for each $k \geq 0$ there is an induced map $H_k(i) : H_k(L) \rightarrow H_k(K)$.

A **persistence module** M consists of \mathbb{Z}_2 -vector spaces M_i for $1 \leq i \leq n$ and linear maps $M_{i \leq j} : M_i \rightarrow M_j$ for $1 \leq i \leq j \leq n$ such for each i , $M_{i \leq i}$ is the identity map and for $1 \leq i \leq j \leq k \leq n$, $M_{j \leq k} \circ M_{i \leq j} = M_{i \leq k}$. A map of persistence modules $\varphi : M \rightarrow N$ consists of linear maps $\varphi_i : M_i \rightarrow N_i$ for $1 \leq i \leq n$ such that $N_{i \leq j} \circ \varphi_i = \varphi_j \circ M_{i \leq j}$ for all $1 \leq i \leq j \leq n$. The category of persistence modules is an abelian category, so we have direct sums of persistence modules (defined elementwise) and maps of persistence modules have images, kernels, and cokernels (also defined elementwise).

Given an interval I in $(\{1, \dots, n\}, \leq)$, let χ_I denote the persistence module given by $(\chi_I)_k = \mathbb{Z}_2$ if $k \in I$ and 0 otherwise and the linear maps in the persistence module are identity maps wherever possible. χ_I is called the interval module supported on the interval I . The **barcode of a persistence module** M is a collection of intervals or **bars** $\{I_j\}_{j=1}^N$ such that $M \cong \bigoplus_{j=1}^N \chi_{I_j}$. The barcode is unique up to reordering. We sometimes denote the bar $[i, j]$ by $[i, j+1]$.

B More detailed definitions

For inclusion of our filtered simplicial complexes $\iota : L \hookrightarrow K$ and each $k \geq 0$ we have persistence modules $C_k(L)$ and $C_k(K)$ and induced maps of persistence modules $d_k : C_k(L) \rightarrow C_{k-1}(L)$, $d_k : C_k(K) \rightarrow C_{k-1}(K)$ and $C_k(\iota) : C_k(L) \hookrightarrow C_k(K)$. For each $k \geq 0$ we also have persistence modules $Z_k(L)$, $B_k(L)$, $Z_k(K)$, $B_k(K)$, $H_k(L)$ and $H_k(K)$ and induced maps of persistence modules $Z_k(\iota) : Z_k(L) \rightarrow Z_k(K)$, $B_k(\iota) : B_k(L) \rightarrow B_k(K)$ and $H_k(\iota) : H_k(L) \rightarrow H_k(K)$. The latter is given by the following commutative diagram of vector spaces and linear maps.

The persistent homology vector spaces [11] of the persistence module $H_k(L)$ are given by $\text{im}((H_k(L))_{i \leq j}) = \frac{Z_k(L_i)}{B_k(L_j) \cap Z_k(L_i)}$, for $1 \leq i \leq j \leq n$. The image persistent homology vector spaces [7] are the persistent homology vector spaces of the persistence module given by the image of $H_k(\iota)$. For $1 \leq i \leq j \leq n$, $\text{im}((\text{im}(H_k(\iota)))_{i \leq j}) = \frac{Z_k(L_i)}{B_k(K_j) \cap Z_k(L_i)}$.

C Proof of algorithm correctness

We prove the correctness of the main algorithm.

► **Theorem 14** (Mixup Decomposition Theorem). *The algorithm in Algorithm 2 returns a correct mixup barcode of $L \hookrightarrow K$.*

Proof. The matrix BL is a submatrix of BK so that the common columns correspond to the same simplices in L . Additionally, reordering the rows in BK sets it up for image persistence

computations, as explained above. Therefore reducing BL and BK using Algorithm 1 yields the persistent homology of L and the image persistence of $L \hookrightarrow K$ respectively.

Specifically, each index of a k -simplex σ with $BL[\sigma] = 0$ corresponds to a unique homology class γ in $H_k(L)$, namely the class *created* by the simplex σ . (We remark that $BL[\sigma] = 0$ implies that the boundary of σ is also a cycle, and hence gives birth to a homology class in degree k .) Whenever τ and τ' exist, each is unique since each reduced matrix is guaranteed to have unique pivots [11]. In particular, they do not depend on the variant of the reduction algorithm, order of column additions, etc. If τ or τ' may not exist, in the case of homology classes persisting forever, which we handle in a straightforward way.

By construction, the pair (σ, τ) is an index persistence pair arising from L and τ is the simplex that destroys γ . As for (σ, τ') there are two options: (1) it is the index *image* persistence pair arising from $L \hookrightarrow K$ [7] and τ' is the index of the simplex that gives premature death to the image of γ in $H_k(K)$; or (2) it coincides with (σ, τ) which corresponds to γ dying immediately in $H_k(K)$.

Therefore each triple (σ, τ', τ) encodes the decomposition of the index persistence bar into the index image persistence sub-bar (σ, τ') and sub-bar (τ', τ) , which we call a mixup sub-bar. \blacktriangleleft

D Multi layer perceptron

A model is trained on vectors and their correct labels to correctly predict labels of previously unseen vectors. The training uses data encoded as vectors, along with their correct integer labels. Assuming there are l unique labels, label j is encoded as the j -th standard basis vector in \mathbb{R}^l . The predicted numerical label is computed from the (soft) prediction vector $p \in \mathbb{R}^l$ as $\arg \max_i p_i$.

This particular model performs computations in **layers**: the output of the current layer is the input to the next layer. The output of the last layer is interpreted as the prediction vector. The i -th layer can be viewed as a function $L_i : \mathbb{R}^n \rightarrow \mathbb{R}^m$, $L_i(v) = f_i(W_i v)$, where W_i is a real matrix. Except for the first and last layer, the dimensions n, m can be freely configured but remain fixed during training. The entries of these matrices serve as trainable parameters and are initialized randomly.

The function f_i is a component-wise nonlinear function, typically called an activation function. Nowadays, a common choice is the ReLU [13, 19] function, which simply returns $\max(0, x)$ at each coordinate. For simplicity, we will use the identity function as the activation for the last layer.

In more geometric terms, each layer performs a linear transformation followed by a projection onto the positive orthant of \mathbb{R}^m , for some m .

Another important choice is the loss function. It evaluates the quality of predictions against the correct labels. The training aims at minimizing this function with respect to the parameters. We use the once-standard **mean squared error loss**. Its geometric counterpart is the **squared Euclidean distance**, which we now use when computing the mixup barcodes as opposed to the usual Euclidean distance.

E Datasets

MNIST. This is a standard dataset, containing 60,000 grayscale images of size 28×28 depicting handwritten decimal digits. It is a heavily preprocessed version of real-world images,

so that the Euclidean distance between two images closely corresponds to their perceptual dissimilarity. For this reason, representing the images as a (labeled) point cloud in \mathbb{R}^{784} yields a faithful representation of the data. It comes split into 50,000 training images, and 10,000 test images. We normalize the vectors so that the values are between 0 and 1. The model achieves 99% test accuracy when trained and tested on the images with labels 0,1 and 2, which we then use for our experiments. These are images of handwritten zeros, ones and twos. We know it managed to disentangle the data well from the visualization in Figure 5, so we expect to see low mixup at the end of training. We are however curious about the higher-dimensional embeddings coming from the remaining layers.

CIFAR10. Another standard dataset, containing 50,000 color photos of size 32×32 depicting various objects, animals etc. We treat this data as a (labeled) point cloud in \mathbb{R}^{3072} , but the Euclidean distance fails to capture the perceptual similarity. We expect to see more significant entanglement between different classes. This dataset is quite challenging for a basic MLP which achieves only 76% test accuracy when trained and tested the images with labels 0,1 and 2. These are images of airplanes, cars and birds. We expect it to fail to disentangle the data, especially differentiating between airplanes and birds may be hard due to similar backgrounds.